Check for updates

Donor–acceptor polymers containing thiazole-fused benzothiadiazole acceptor units for organic solar cells†

Tomoya Nakamura,[a] Yasuhisa Ishikura,[a] Noriko Arakawa,[a] Megumi Hori,[a] Motoi Satou,[a] Masaru Endo,[a] Hisashi Masui,[b] Shinichiro Fuse,[c] Takashi Takahashi,[b] Yasujiro Murata, [ID][a] Richard Murdey [ID][a] and Atsushi Wakamiya [ID] *[a]

Two p-type semiconducting donor–acceptor polymers were designed and synthesized for use in organic solar cells. The polymers combine a benzodithiophene (BDT) donor and a thiazole-fused benzothiadiazole (TzBT) acceptor. Two TzBT acceptor units are compared, one with an alkylthio group (**P1**) and the other with a more strongly electron-withdrawing alkylsulfonyl group (**P2**) at the fused thiazole ring. The strongly electron-accepting nature of the TzBT unit lowers the lowest unoccupied molecular orbital (LUMO) energy of **P1** and **P2** relative to that of the BT analog (**PBDT-BT**), without altering the energy of the highest occupied molecular orbital (HOMO). Despite the smaller optical band gaps, bulk heterojunction organic solar cells fabricated using these polymers in a PC$_{71}$BM blend showed high open-circuit voltages. The power conversion efficiency (PCE) of the **P1**-based device reached 6.13%. Though efficiency of the **P2**-based device was lower, photoelectric conversion extended into the near-IR region up to 950 nm.

[a]Institute for Chemical Research, Kyoto University, Gokasho, Uji, Kyoto 611-0011, Japan. E-mail: wakamiya@scl.kyoto-u.ac.jp

[b]Department of Pharmaceutical Sciences, Yokohama University of Pharmacy, 601, Matano-cho, Totsuka-ku, Yokohama 245-0066, Japan

[c]Laboratory for Chemistry and Life Science, Institute of Innovative Research, Tokyo Institute of Technology, 4259 Nagatsuta-cho, Midori-ku, Yokohama, Kanagawa 226-8503, Japan

† Electronic supplementary information (ESI) available: Thermogravimetric analysis, Tauc plots, cyclic voltammetry, theoretical calculations, thin film absorption spectra, atomic force microscopy images, photovoltaic characterization, space-charge limited current measurements, and NMR spectra. See DOI: 10.1039/c9ra00229d
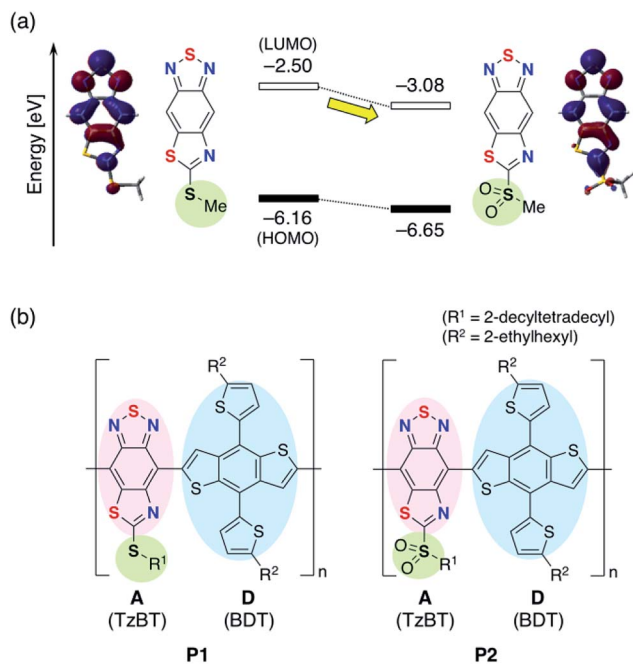
Introduction

Organic solar cells (OSCs) have attracted considerable attention as low cost, flexible, and light-weight sources of electrical power.[1–4] In bulk-heterojunction OSC devices, p-type materials, typically semiconducting polymers, are blended with n-type molecular materials, typically fullerene derivatives such as [6,6]-phenyl-C$_{71}$-butyric acid methyl ester (PC$_{71}$BM).[5,6] The p-type semiconductor is often a conjugated donor–acceptor (D–A) polymer consisting of alternating electron-rich donor units and electron-deficient acceptor units.[7,8] A promising approach to improve the power conversion efficiency (PCE) of OSCs is using p-type materials with a narrow highest occupied molecular orbital (HOMO)–lowest unoccupied molecular orbital (LUMO) band gap (E_g) to increase short-circuit current density (J_{SC}).[9] The open circuit voltage, V_{OC}, scales closely with the energy difference between the HOMO of the p-type polymer and LUMO of the n-type fullerene.[10] Hence, lowering the LUMO energy level of the p-type polymer without changing the HOMO energy level should lead to a narrow band gap without sacrificing the V_{OC}. The development of strong acceptor units is therefore a key element for fine-tuning the electronic structure. The difference in energy between the optical band gap of the absorber and the open-circuit voltage of the device is defined as the photon energy loss ($E_{loss} = E_g - eV_{OC}$).[11–13] For high PCE, the photon energy loss should be minimized.

2,1,3-Benzothiadiazole (BT) is a widely used acceptor unit in D–A polymers.[14–16] The strong electron-accepting ability of benzothiadiazole stems from the strong butadiene character and the presence of the two electron-withdrawing C=N double bonds. A common approach to enhance the electron-accepting ability is the introduction of electron-withdrawing substituents such as fluoro,[17–19] chloro,[20] and cyano[21] groups. As a unique electronic modification, we have demonstrated the utility of the formation of intramolecular B–N bonds, which makes it possible to lower the LUMO energy level without changing the orbital distribution.[22–29] Another way for modification of BT unit is the heteroannulation at the 5- and 6-positions to give acceptors such as thiadiazoloquinoxaline (TDQ) and benzobisthiadiazole (BBT).[30,31] We have recently developed a thiazole-fused BT skeleton (TzBT) as a new type of electron acceptor unit with further enhancement of the electron-accepting ability of BT skeleton.[32–34] Additional tuning of the electron-accepting character is realized by changing the alkylthio group to

Results and discussion
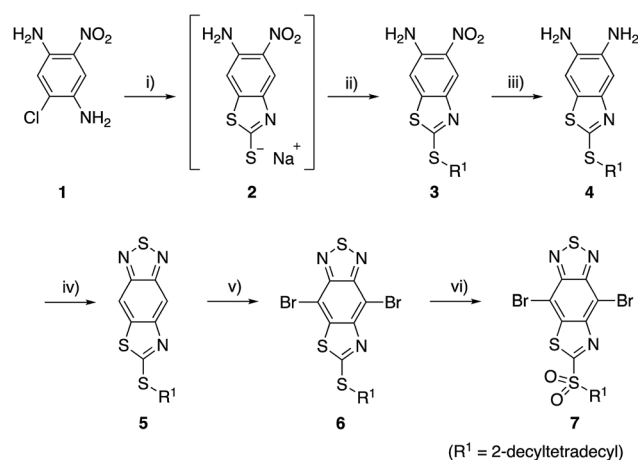
Synthesis and characterization of polymers

For the synthesis of TzBT acceptor unit, we followed the same method we previously developed for the synthesis of the unit with a methylthio group substituent (Scheme 1).[34] The reaction of commercially available 2-chloro-5-nitrobenzene-1,4-diamine (**1**) with sodium ethylxanthate gave the intermediate **2**, which was treated with 2-decyltetradecyl bromide to give benzothiazole **3** in 68% yield in two steps. Reduction of the nitro group by tin(II) chloride gave diamine **4**, and the following condensation with thionyl chloride gave thiazole-fused BT **5** in 81% yield in two steps. The reaction of **5** with bromine in the presence of iron(III) chloride yielded **6** with an alkylthio group in 63% yield. Furthermore, **7** with an alkylsulfonyl group was synthesized by the reaction with two equivalents of mCPBA in 89% yield.

The monomers **6** and **7** were polymerized with the benzodithiophene (BDT) unit via the Stille coupling reaction assisted by microwave heating to give **P1** and **P2**, respectively (Scheme 2). The number-average molecular weight (M_n) and weight-average molecular weight (M_w) were estimated to be 16 kDa and 35 kDa with a polydispersity index (PDI) of 2.15 for **P1** by high-temperature gel permeation chromatography (GPC) using o-dichlorobenzene as the eluent at 140 °C. M_n and M_w were 22 kDa and 66 kDa with a PDI of 3.04 for **P2** (Table 1).

The thermal stability of the polymers was examined by thermogravimetric analysis (TGA) under nitrogen atmosphere with a heating rate of 10 °C min^{-1} (Fig. S1†). The 5% weight loss temperatures (T_{d5}) were 332 °C and 340 °C for **P1** and **P2**, respectively, confirming that these polymers have good thermal stability.

Photophysical properties

The UV-Vis-NIR absorption spectra of the polymers were measured in dichloromethane solution and in the solid state

Fig. 1 (a) Fine-tuning of electron-accepting ability in TzBT bearing alkylthio group. Calculated energy level diagram with depictions of the LUMO at B3LYP/6-31G(d) level of theory.[37] (b) Chemical structures of TzBT-based D–A polymers **P1** and **P2**.

alkylsulfonyl (Fig. 1a).[34] We anticipated that this simple substitution of the alkylthio group in the TzBT derivative can fine-tune the electronic structure of a D–A polymer when TzBT is used as the acceptor unit.

Wong, Jones, and co-workers reported a D–A polymer composed of a benzodithiophene (BDT) donor and a BT acceptor (**PBDT-BT**) for the use as a p-type semiconductor in OSC devices with a blend with PC$_{71}$BM.[35,36] Although a high PCE of 9.4% is reported, the device shows a relatively large photon energy loss of 0.83 eV as a result of the high-lying LUMO energy level of **PBDT-BT**. The PCE might therefore be further improved by reducing the band gap of the polymer while maintaining the V_{OC}. To examine the potential of the TzBT unit in OSC devices, we designed donor–acceptor polymers containing two types of TzBT acceptor units, **P1** with alkylthio groups and **P2** with alkylsulfonyl groups at the fused thiazole rings, respectively (Fig. 1b). The strong electron-accepting nature of TzBT unit, especially in the unit with alkylsulfonyl substituent, is expected to lower the LUMO energy levels in these polymers compared to the BT analog, resulting in a smaller photon energy loss (E_{loss}).

In the present work, the synthesis of the D–A polymers is reported, followed by a summary of the photophysical properties evaluated by ultraviolet-visible-NIR (UV-Vis-NIR) spectroscopy and photoemission yield spectroscopy (PYS). Smaller optical band gaps compared to BT-based polymers were observed, and PYS confirmed that the HOMO energy levels are relatively unchanged. Bulk heterojunction organic solar cell devices were fabricated using the blend of these polymers with PC$_{71}$BM as the light-absorbing layer. **P1** and **P2**-based devices exhibited smaller photon energy losses than that for **PBDT-BT** based device.

Scheme 1 Synthesis of thiazole-fused BT units. Reagents and conditions: (i) sodium ethylxanthate (2.0 equiv.), DMF, 120 °C, 3 h; (ii) R^{1}Br (1.5 equiv.), DMF, 0 °C to rt, 16 h, 68% in two steps; (iii) SnCl$_2$·2H$_2$O (5.0 equiv.), MeOH/HCl aq., 70 °C, 22 h; (iv) SOCl$_2$ (3.0 equiv.), Et$_3$N (6.0 equiv.), CH$_2$Cl$_2$, 0 °C to rt, 2 h, 81% in two steps; (v) Br$_2$ (48 equiv.), FeCl$_3$·6H$_2$O (0.6 equiv.), 50 °C, 19 h, 63%; (vi) mCPBA (2.0 equiv.), CH$_2$Cl$_2$, rt, 28 h, 89%.
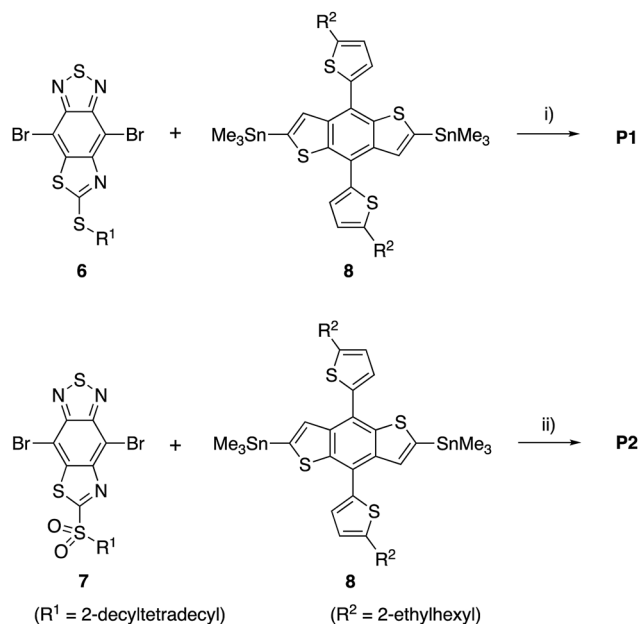
Scheme 2 Synthesis of D−A polymers. Reagents and conditions: (i) Pd$_2$(dba)$_3$·CHCl$_3$ (2 mol%), P(o-tolyl)$_3$ (8 mol%), toluene, microwave, 160 °C (ca. 3.4 atm), 1 h, 86%; (ii) Pd$_2$(dba)$_3$·CHCl$_3$ (2 mol%), P(o-tolyl)$_3$ (8 mol%), toluene, microwave, 160 °C (ca. 3.4 atm), 1 h, 69%.

(R^1 = 2-decyltetradecyl)   (R^2 = 2-ethylhexyl)

Table 1 Characterization of polymers

Polymer	M_n^a [kDa]	M_w^a [kDa]	PDI^a	DP$_n^b$	T_{d5}^c [°C]
P1	16.2	34.8	2.15	14.2	332
P2	21.5	65.5	3.04	18.4	340

^{a} Determined by GPC using polystyrene standard and o-dichlorobenzene as the eluent. ^{b} Degree of polymerization based on the repeating unit. ^{c} 5% weight loss temperature.

(Fig. 2). In solution, **P1** with alkylthio substituents shows an absorption maximum ($\lambda_{\max}$) at 746 nm. This value is red-shifted compared to that of the BT analog, **PBDT-BT** ($\lambda_{\max}$ = 650 nm),[35,36] by *ca.* 100 nm, as a result of the enhanced electron-accepting nature of the TzBT unit. **P2** with alkylsulfonyl substituents exhibits $\lambda_{\max}$ of 829 nm in the near-IR region, which is further red-shifted by *ca.* 80 nm compared to that of **P1**. In the thin films, the absorption is broadened and red-shifted to 756 nm for **P1** and 848 nm for **P2**, respectively, suggesting some degree of intermolecular interactions in the solid state.

The optical band gaps (E_g) were estimated using Tauc plots of the solid state absorption spectra (Fig. S2†). E_g of **P1** and **P2** are 1.54 eV and 1.37 eV, respectively, which are smaller than that of **PBDT-BT** (1.75 eV).

Electronic properties

In this section, the solid state energy levels of these polymers as well as n-type PC$_{71}$BM are determined by experimental and theoretical methods. The HOMO energy level (E_{HOMO}) of the polymer thin films on ITO substrates was estimated using photoemission yield spectroscopy (PYS) in air. E_{HOMO} of n-type
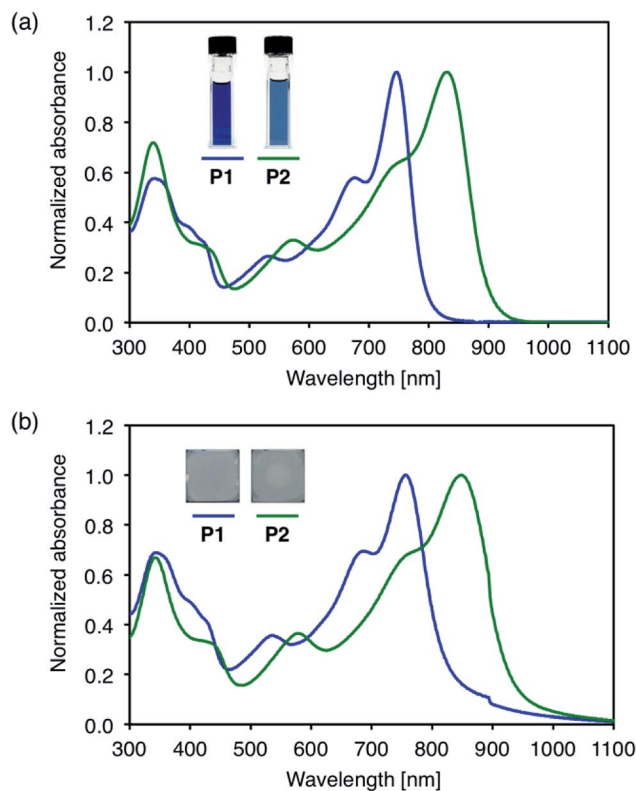

Fig. 2 UV-Vis absorption spectra of D−A polymers; (a) in CH$_2$Cl$_2$ solution and (b) in the solid state.

PC$_{71}$BM was also investigated. The values of −5.26 eV, −5.35 eV, and −6.08 eV were obtained for **P1**, **P2**, and PC$_{71}$BM, respectively (Fig. 3a). The E_{HOMO} values of **P1** and **P2** do not significantly differ from the value of **PBDT-BT** (−5.27 eV) estimated similarly by PYS.[35] The LUMO energy levels (E_{LUMO}) were determined as the sum of E_{HOMO} and E_g. The values were −3.72 eV, −3.98 eV, and −4.19 eV for **P1**, **P2**, and PC$_{71}$BM, respectively. Compared to the E_{LUMO} of **PBDT-BT** (−3.52 eV),[35] the E_{LUMO} of **P1** and **P2** were found to be deeper by 0.20 eV and 0.46 eV, respectively. The lowering of LUMO energy levels in TzBT-based polymers was also confirmed by cyclic voltammetry (CV) measurements (Fig. S3†). As the energetic parameters determined by CV measurements can be affected by the solvent, supporting electrolyte, and electrodes,[38] the parameters determined by PYS and E_g are considered to be more reliable. Fig. 3b shows the energy level diagram of **P1**, **P2**, and PC$_{71}$BM, together with the energy levels of **PBDT-BT**[35] estimated by PYS and the optical band gap. Table 2 summarizes the physicochemical properties. As a result of the effective lowering of the LUMO energy levels in **P1** and **P2**, the energy differences in the LUMO energy of p-type polymers and PC$_{71}$BM decrease from 0.67 eV for **PBDT-BT** to 0.47 eV for **P1** and 0.21 V for **P2**, respectively. Consequently, smaller photon energy losses are anticipated in organic solar cells using these TzBT-based polymers, especially in the cells using **P2** with alkylsulfonyl groups.

The DFT calculations on the tetramer model compounds clarifies the selective reduction in the LUMO energy levels in these polymers. The calculated electron density of the LUMO is
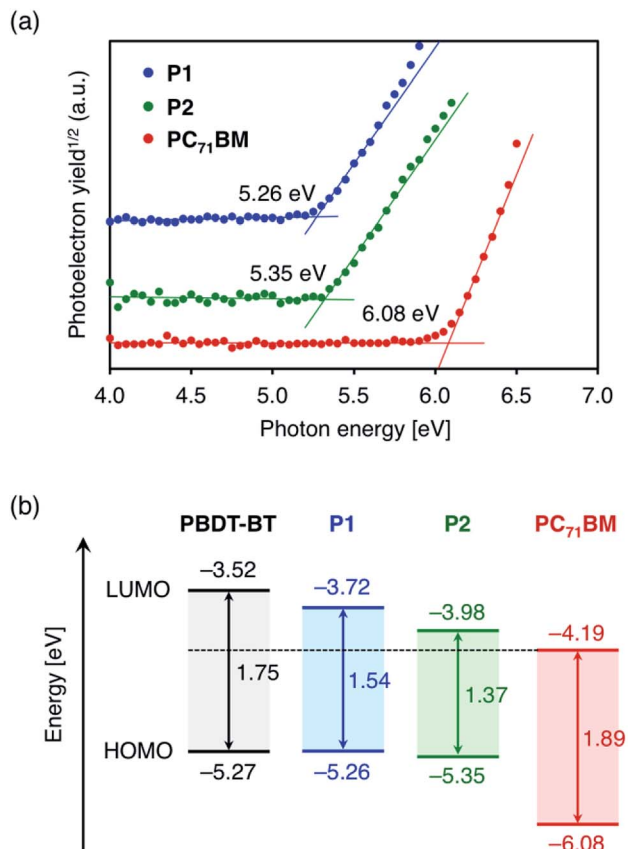
(a)

(b)

Fig. 3 (a) Photoemission yield spectra of the polymers as well as PC$_{71}$BM in the solid state and (b) energy level diagram of **P1**, **P2**, and PC$_{71}$BM, estimated from photoemission yield spectroscopy and optical band gap in the solid state. Energy levels of **PBDT-BT**[35] are also shown for comparison.

located on the TzBT moieties, whereas the HOMO is mainly distributed at the BDT donor units (Fig. S4†). The use of a strong acceptor unit should therefore have a greater impact on the LUMO energy than the HOMO energy.

Device fabrication and photovoltaic properties

To evaluate the photovoltaic properties of these TzBT-based polymers, bulk heterojunction solar cells using the two polymers were prepared with the following structure; indium tin

Table 2 Physicochemical properties of polymers

Polymer	λ_{max}[a] [nm]		E_{HOMO}[b] [eV]	E_g[c] [eV]	E_{LUMO}[d] [eV]
	Solution	Film			
P1	746	756	−5.26	1.54	−3.72
P2	829	848	−5.35	1.37	−3.98

[a] Absorption maximum. [b] The HOMO energy levels estimated by photoemission yield spectroscopy (PYS) in air. [c] Optical band gap estimated from the edge of the Tauc plot. [d] The LUMO energy levels calculated from the HOMO energy level and optical band gap (E_{LUMO} = E_{HOMO} + E_g).

oxide (ITO)/zinc oxide (ZnO)/polymer : PC$_{71}$BM/molybdenum oxide (MoO$_x$)/Ag. The light-absorbing layer was spin-coated from the polymer : PC$_{71}$BM blend solution (optimized ratio, 1 : 1.2 wt/wt for **P1**, 1 : 1 wt/wt for **P2**) in chlorobenzene with 3 vol% 1,8-diiodooctane (DIO) as an additive to control the bulk heterojunction morphology.[39] The optimal thickness of the light-absorbing layer was 80 nm, similar to the BT analog **PBDT-BT** device (90 nm).[35]

Fig. 4a shows the current density–voltage (J–V) characteristics of the representative polymer : PC$_{71}$BM cells under AM 1.5 G irradiation (100 mW cm^{-2}). The solar cell devices using **P1** and **P2** showed high open-circuit voltages (V_{OC}) of 0.78 V and 0.79 V, respectively (Table 3). The high V_{OC} of the cell using **P2** with alkylsulfonyl substituents is especially striking given the small band gap of **P2**. From the optical band gaps of these polymers (1.54 eV for **P1** and 1.37 eV for **P2**), the photon energy losses (E_{loss} = E_g − eV_{OC}) were estimated to be 0.76 eV and 0.58 eV for **P1** and **P2**-based cells, respectively. The energy losses are lower compared to that for the BT analog **PBDT-BT** (0.83 eV) by 0.06 eV and 0.25 eV for **P1** and **P2**, respectively.[35] The reduced energy loss is attributed to the enhanced electron-accepting ability of the TzBT units, which lowers the LUMO energy levels of D–A polymers.

The PCEs of the **P1** and **P2**-based devices were 6.13% and 1.15%, respectively (Table 3). The lower PCEs than the reported
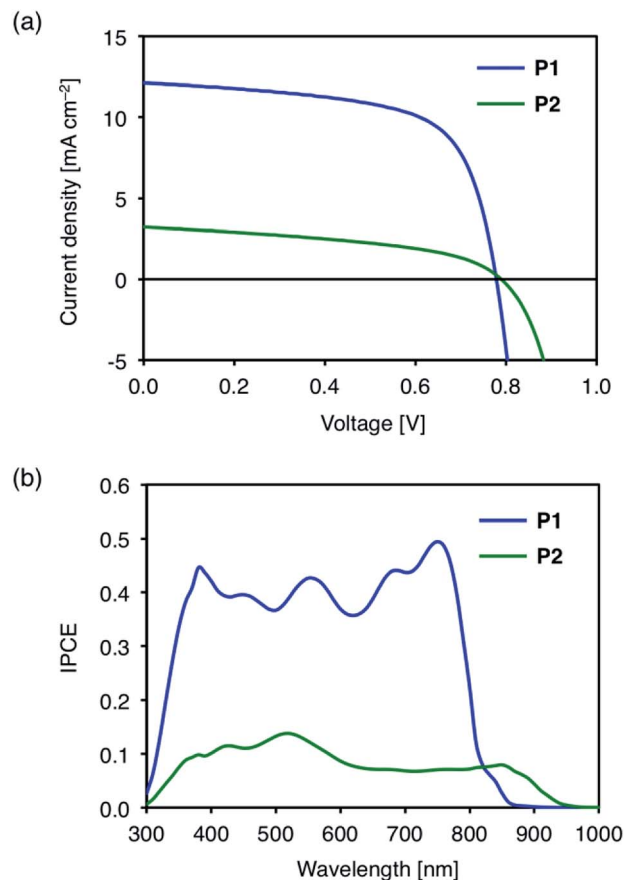
(a)

(b)

Fig. 4 (a) J−V characteristics, and (b) incident photon to current conversion efficiency (IPCE) spectra of polymer/PC$_{71}$BM cells.

Table 3 Photovoltaic parameters of polymer/PC$_{71}$BM Cells

Polymer	J_{SC} [mA cm^{-2}]	V_{OC} [V]	FF	PCE [%]	$E_{loss}{}^a$ [eV]
P1	12.1	0.78	0.65	6.13 (5.97 ± 0.21)^b	0.76
P2	3.2	0.79	0.45	1.15 (1.12 ± 0.03)^c	0.58

^{a} Photon energy loss defined by $E_{loss} = E_g - eV_{OC}$. ^{b} Average PCE with standard deviation from 15 independent devices. ^{c} Average PCE with standard deviation from 6 independent devices.

value for the **PBDT-BT** based cell (9.4%) are mainly due to the lower short-circuit current densities (J_{SC}) of 12.1 mA cm^{-2} and 3.2 mA cm^{-2} for the **P1** and **P2**-based devices, respectively, compared to 15.4 mA cm^{-2} for the **PBDT-BT** based device. The reduced current output correlates with the lower incident photon to current conversion efficiencies (IPCE) of **P1** (0.4–0.5) and **P2** (*ca.* 0.1) based devices (Fig. 4b) compared to the **PBDT-BT** based device (0.6–0.8).[35] The IPCE spectra closely resemble the thin film absorption spectra of the polymer : PC$_{71}$BM blends (Fig. S5†). Though the IPCE of **P2**-based device was low, it should be noted that the photon to current conversion in the near-IR region extends up to 950 nm.

The different IPCE and J_{SC} values could be caused by at least three different factors: (i) the morphology of polymer : PC$_{71}$BM heterojunction, (ii) the charge carrier mobility of the blends, or (iii) the energy offset of the LUMOs between the polymer and PC$_{71}$BM. These possibilities were examined as follows:

The film morphology of polymer and PC$_{71}$BM blends was imaged by atomic force microscopy (AFM). Without 1,8-diiodooctane (DIO) additive, the films of **P1** : PC$_{71}$BM exhibits large-size phase separation with isolated PC$_{71}$BM domains of *ca.* 300 nm (Fig. S6a†). The addition of 3 wt% DIO significantly decreased phase separation size to *ca.* 100 nm (Fig. S6b†). This observation is in good agreement with the increased J_{SC} in the **P1**-based device with increased amount of DIO additive (Fig. S7 and Table S1†). The phase separation size is, however, still larger than the ideal value of ~20 nm, which is likely the reason of the moderate IPCE and J_{SC} of **P1**-based device. Though the **P2** : PC$_{71}$BM blends have slightly smaller domain size of *ca.* 80 nm (Fig. S6d†), the overall morphology is similar, making it difficult to assign any causal relationship between morphology and performance.

The hole mobility of the polymer : PC$_{71}$BM blends was measured using the space-charge-limited current (SCLC) method. Hole only devices were fabricated with the structure of ITO/poly(3,4-ethylenedioxythiophene) polystyrene sulfonate (PEDOT:PSS)/polymer : PC$_{71}$BM/Au. Both polymers exhibit similar hole mobility, which was $(1.06 \pm 0.09) \times 10^{-5}$ cm^2 V^{-1} s^{-1} for **P1** and $(1.21 \pm 0.08) \times 10^{-5}$ cm^2 V^{-1} s^{-1} for **P2** (Fig. S8 and Table S2†). It seems then that hole mobility is also unlikely a limiting factor in the present instance.

As no significant differences were observed in **P1** and **P2** in regard to film morphology and hole mobility, it would be reasonable to ascribe the different J_{SC} values to the energy offsets in the LUMOs of the polymer and PC$_{71}$BM. Whereas the energy offset is 0.47 eV for **P1**, it is only 0.21 eV for **P2**, the latter being smaller than the empirical value of 0.3 eV considered

necessary for efficient charge separation.[10] This would explain why the **P2**-based device shows low J_{SC}.

Conclusions

Two donor–acceptor polymers combining a thiazole-fused benzothiadiazole (TzBT) acceptor unit with the benzodithiophene (BDT) donor unit were designed and synthesized. In polymer **P1**, the TzBT acceptor unit had an alkylthio substituent. In polymer **P2**, this was replaced with a more electron-withdrawing alkylsulfonyl group. The strong electron-accepting nature of the TzBT units lowered the LUMO energy levels of **P1** and **P2** compared to that of the BT analog (**PBDT-BT**) by 0.20 and 0.46 eV, respectively. Since the HOMO energies were remained largely unchanged, the band gaps were reduced. Bulk heterojunction organic solar cells using a polymer/PC$_{71}$BM blend showed high V_{OC} of 0.78 V and 0.79 V for **P1** and **P2**-based devices, despite their small optical band gaps of 1.54 eV and 1.37 eV. The photon energy loss was determined to be 0.76 eV and 0.58 eV, respectively, smaller than for the **PBDT-BT** based device (0.83 eV). The overall power conversion efficiencies of these devices were found to be 6.13% for **P1** and 1.15% for **P2**. NIR photon-to-current conversion was found to extend to 860 nm for **P1** and 950 nm for **P2**.

Experimental section

General

Melting points (mp) were measured on a Yanaco Micro Melting Point Apparatus or Stanford Research Systems Opti Melt. ^{1}H and ^{13}C NMR spectra were recorded with JEOL JNM ECA500 (500 MHz for ^{1}H and 126 MHz for ^{13}C). Chemical shifts are reported in δ ppm using residual protons in the deuterated solvents for ^{1}H NMR and using solvent peaks for ^{13}C NMR as internal standards. UV-Vis-NIR absorption spectra were recorded with a Shimadzu UV-3150 spectrometer. Mass spectra were measured on a Bruker micrOTOF-Q II (APCI). Ionization potentials in the solid states were determined by an ambient photoelectron spectroscopy method with a Riken-Keiki AC-3 spectrometer. Thermogravimetric analysis (TGA) was performed on a SHIMADZU TGA-50 apparatus. Thin layer chromatography (TLC) was performed on plates coated with 0.25 mm thick silica gel 60F-254 (Merck). Column chromatography was performed using silica gel PSQ 60B (Fuji Silysia) or PSQ 100B (Fuji Silysia). The microwave reaction was performed using Anton Paar Monowave 300. All reactions were carried out under an argon atmosphere except as otherwise noted.

Analytical GPC was performed on a HLC 8120 GPC system with a TOSOH TSKgel GMHHR-H(S)HT column. *o*-Dichlorobenzene was used as the mobile phase with a flow rate of 1.0 mL min^{-1} at 140 °C. The columns were calibrated against nine standard polystyrene samples (M_n = 1200–1 410 000).

Photocurrent-voltage measurements for organic solar cells were measured in air with an OTENTO-SUNIII (BUNKOUKEIKI Co., Ltd.) and a Keithley 2400. The light intensity of the illumination source was adjusted by using standard silicon

photodiodes: BS520 for *J–V* characteristics and SiPD S1337-1010BQ for EQE measurements.

All calculations were conducted using the Gaussian 09 program.[37] The geometries were optimized at the B3LYP/6-31G(d) level of theory. The fact that these geometries are at the energy minimum was confirmed by frequency calculations at the same level of theory.

Synthesis

2-(2-Decyltetradecylthio)-5-nitro-1,3-benzothiazole-6-amine (3).

To a 1 L two-necked flask were added 2-chloro-5-nitrobenzene-1,4-diamine (**1**) (9.00 g, 48.0 mmol), sodium ethylxanthate (13.8 g, 96.0 mmol), and dry DMF (480 mL). The mixture was stirred at 120 °C for 3 h and then cooled in an ice bath. 2-Decyltetradecylbromide (29.9 g, 71.8 mmol) was then added dropwise over 10 min. The mixture was allowed to warm to room temperature and was stirred for 16 h. The reaction mixture was concentrated under reduced pressure and then water (300 mL) was added. The aqueous phase was extracted with ether (200 mL × 3). The combined organic layers were washed with saturated NaCl aq., dried over Na_2SO_4, and then concentrated under reduced pressure. The crude product was purified by silica gel column chromatography (toluene/hexane = 2 : 1, R_f = 0.25) to give **3** (18.3 g, 68% in two steps) as dark red oil.

^{1}H NMR (500 MHz, $CDCl_3$): δ 8.55 (s, 1H), 7.08 (s, 1H), 5.97 (brs, 2H), 3.36 (d, J = 5.7 Hz, 2H), 1.77–1.82 (m, 1H), 1.25–1.43 (m, 40H), 0.86–0.89 (m, 6H); ^{13}C NMR (126 MHz, $CDCl_3$): δ 166.7, 145.5, 145.0, 141.2, 132.2, 117.7, 108.2, 38.2, 37.6, 33.2 (2C), 31.9 (2C), 29.8 (2C), 29.6 (8C), 29.3 (2C), 26.5 (2C), 22.7 (2C), 14.1 (2C); HRMS (APCI) (*m/z*): [M − H]− calcd. for $C_{31}H_{52}N_3O_2S_2$, 562.3506; found, 562.3506.

6-(2-Decyltetradecylthio)thiazolo[5,4-*f*]-2,1,3-benzothiadiazole (5).

To a 2 L two-necked flask were added **3** (18.3 g, 32.5 mmol), $SnCl_2 \cdot 2H_2O$ (36.7 g, 162 mmol), MeOH (900 mL), distilled water (90 mL), and HCl aq. (1 M, 16.2 mL, 16.2 mmol). The mixture was stirred at 70 °C for 22 h. The reaction mixture was concentrated under reduced pressure and then neutralized with saturated $NaHCO_3$ aq. (300 mL). 2 M NaOH aq. (*ca.* 200 mL) was added and the aqueous phase was extracted with CH_2Cl_2 (200 mL × 3). The combined organic layers were washed with saturated NaCl aq. (300 mL), dried over Na_2SO_4, filtered, and concentrated under reduced pressure to give **4** as pale brown solids. Triethylamine (23.7 mL, 170 mmol) was added to a solution of **4** in CH_2Cl_2 (500 mL) in a 1 L two-necked flask and the mixture was cooled in an ice bath. Then, $SOCl_2$ (6.16 mL, 85.0 mmol) was added dropwise over 12 min. The mixture was allowed to warm to room temperature and was stirred for 2 h. The resulting mixture was neutralized with sat. $NaHCO_3$ aq. (300 mL) and the aqueous phase was extracted with CH_2Cl_2 (100 mL × 3). The combined organic layers were washed with saturated NaCl aq. (200 mL), dried over Na_2SO_4, filtered, and concentrated under reduced pressure. The crude product was purified by silica gel column chromatography (toluene/hexane = 2 : 1, R_f = 0.25) to give **5** (14.0 g, 81% in two steps) as brown oil.

^{1}H NMR (500 MHz, $CDCl_3$): δ 8.32 (s, 1H), 8.29 (s, 1H), 3.47 (d, J = 6.3 Hz, 2H), 1.83–1.87 (m, 1H), 1.24–1.46 (m, 40H), 0.85–0.89 (m, 6H); ^{13}C NMR (126 MHz, $CDCl_3$): δ 172.9, 155.8, 153.9, 152.0, 140.6, 111.5, 110.3, 38.1, 37.7, 33.3 (2C), 31.9 (2C), 29.8 (2C), 29.6 (8C), 29.3 (2C), 26.6 (2C), 22.7 (2C), 14.1 (2C); HRMS (APCI) (*m/z*): [M]− calcd for $C_{31}H_{51}N_3S_3$, 561.3245; found, 561.3240; elemental analysis calcd (%) for $C_{31}H_{51}N_3S_3$: C 66.26, H 9.15, N 7.48; found: C 66.05, H 9.26, N 7.50.

4,8-Dibromo-6-(2-decyltetradecylthio)thiazolo[5,4-*f*]-2,1,3-benzothiadiazole (6).

To a 10 mL two-necked flask were added **5** (281 mg, 0.50 mmol) and $FeCl_3 \cdot 6H_2O$ (81 mg, 0.30 mmol). Br_2 (1.24 mL, 24 mmol) was added and the mixture was stirred at 50 °C for 19 h. Saturated $NaHSO_3$ aq. (100 mL) was added to consume the excess bromine. The aqueous phase was extracted with CH_2Cl_2 (50 mL × 2). The combined organic layers were washed with saturated NaCl aq. (50 mL), dried over Na_2SO_4, filtered, and concentrated under reduced pressure. The crude product was purified by silica gel column chromatography (toluene/hexane = 1 : 1, R_f = 0.6) to give **6** (243 mg, 63%) as yellow oil.

^{1}H NMR (500 MHz, $CDCl_3$): δ 3.50 (d, J = 6.3 Hz, 2H), 1.87–1.91 (m, 1H), 1.24–1.46 (m, 40H), 0.85–0.89 (m, 6H); ^{13}C NMR (126 MHz, $CDCl_3$): δ 173.5, 152.6, 152.1, 149.8, 142.9, 102.7, 102.2, 38.6, 38.0, 33.4 (2C), 31.9 (2C), 29.9 (2C), 29.6 (8C), 29.3 (2C), 26.6 (2C), 22.7 (2C), 14.1 (2C); HRMS (APCI) (*m/z*): [M]− calcd for $C_{31}H_{49}Br_2N_3S_3$, 717.1455; found, 717.1471.

4,8-Dibromo-6-(2-decyltetradecylsulfonyl)thiazolo[5,4-*f*]-2,1,3-benzothiadiazole (7).

To a 10 mL two-necked flask were added **6** (217 mg, 0.30 mmol) and dichloromethane (3.0 mL). *m*CPBA (148 mg, 0.60 mmol) was added and the mixture was stirred at room temperature for 28 h. 10% $Na_2S_2O_4$ aq. (20 mL) was added, and the aqueous phase was extracted with CH_2Cl_2 (20 mL × 2). The combined organic layers were washed with saturated NaCl aq. (20 mL), dried over Na_2SO_4, filtered, and concentrated under reduced pressure. The crude product was purified by silica gel column chromatography (toluene/hexane = 2 : 1, R_f = 0.6) to give **7** (201 mg, 89%) as a pale-yellow solid.

Mp (decomp.): 280.6 °C; ^{1}H NMR (500 MHz, $CDCl_3$): δ 3.61 (d, 2H), 2.18–2.21 (m, 1H), 1.21–1.57 (m, 40H), 0.86–0.89 (t, overlapped, 12H); ^{13}C NMR (126 MHz, $CDCl_3$): δ 171.7, 152.3, 151.2, 151.1, 141.8, 110.3, 104.8, 57.8, 33.2 (2C), 32.9, 31.9 (2C), 29.7–29.5 (12C), 26.0 (2C), 22.7 (2C), 14.1 (2C); HRMS (APCI) (*m/z*): [M]− calcd for $C_{31}H_{49}Br_2N_3O_2S_3$, 749.1354; found, 749.1372.

P1. To a 30 mL reaction vessel were added **6** (144 mg, 0.20 mmol), **8** (182 mg, 0.20 mmol), $Pd_2(dba)_3 \cdot CHCl_3$ (4.1 mg, 0.0040 mmol), P(*o*-tolyl)$_3$ (4.9 mg, 0.016 mmol), and dry toluene (10 mL). The vessel was put into a microwave reactor and heated at 160 °C for 1 h. The reaction mixture was poured into methanol (100 mL) and the precipitates were collected by filtration. The low molecular weight fraction was removed by sequential Soxhlet extraction with methanol, acetone, and hexane. The residue was extracted with chloroform and was reprecipitated in methanol. The precipitate was filtered and dried under vacuum to give **P2** (185 mg, 78%) as a dark-blue solid. GPC (DCB, 140 °C): M_n = 16.2 kDa, M_w = 34.8 kDa, PDI = 2.15.

P2. To a 10 mL reaction vessel were added **7** (76 mg, 0.10 mmol), **8** (92 mg, 0.10 mmol), $Pd_2(dba)_3 \cdot CHCl_3$ (2.1 mg, 0.0020

mmol), P(o-tolyl)$_3$ (2.4 mg, 0.0080 mmol), and dry toluene (5 mL). The vessel was put into a microwave reactor and heated at 160 °C for 1 h. The reaction mixture was poured into methanol (50 mL) and the precipitates were collected by filtration. The low molecular weight fraction was removed by sequential Soxhlet extraction with methanol, acetone, and hexane. The residue was extracted with chloroform and was reprecipitated in methanol. The precipitate was filtered and dried under vacuum to give **P2** (82 mg, 69%) as a dark-blue solid. GPC (DCB, 140 °C): $M_n = 21.5$ kDa, $M_w = 65.5$ kDa, PDI = 3.04.

Solar cell fabrication

The ITO-coated glass substrate (5 Ω cm^{-2}, 2.5 cm × 2.5 cm, GEOMATEC) was washed carefully under ultrasonic irradiation using water (15 min), acetone (15 min), detergent solution (Semico Clean 56, Furuuchi chemical, 15 min), water (15 min) and ethanol (15 min). The substrate was further cleaned with a Filgen UV230 UV/ozone cleaner.

0.2 M Zn(OAc)$_2$ solution was prepared by dissolving Zn(OAc)$_2$·2H$_2$O (110 mg, 0.50 mmol) in ethanolamine (30 μL) and anhydrous ethanol (2.5 mL). A thin layer of ZnO was prepared onto the ITO substrate by spin-coating of precursor solution at 1200 rpm for 50 s under relative humidity of 30%. The resulting substrate was heated at 150 °C for 30 min under ambient conditions.

The photoactive layers were deposited in a glove box filled with an inert gas. For **P1**-based device, chlorobenzene solution containing 10 mg mL^{-1} of **P1** with PC$_{71}$BM (**P1** : PC$_{71}$BM = 1 : 1.2 wt/wt) and 3 vol% 1,8-diiodooctane was deposited by spin-coating at 900 rpm for 40 s. For **P2**-based device, chlorobenzene solution containing 5 mg mL^{-1} of **P2** with PC$_{71}$BM (**P2** : PC$_{71}$BM = 1 : 1 wt/wt) and 3 vol% 1,8-diiodooctane was deposited by spin-coating at 900 rpm for 40 s. Finally, a layer of MoO$_x$ (10 nm) and silver (90 nm) were vacuum deposited.

Conflicts of interest

There are no conflicts to declare.

Acknowledgements

Notes and references

1 G. Li, R. Zhu and Y. Yang, *Nat. Photonics*, 2012, **6**, 153–161.

2 M. Kaltenbrunner, M. S. White, E. D. Głowacki, T. Sekitani, T. Someya, N. S. Sariciftci and S. Bauer, *Nat. Commun.*, 2012, **3**, 770.

3 Z. He, B. Xiao, F. Liu, H. Wu, Y. Yang, S. Xiao, C. Wang, T. P. Russell and Y. Cao, *Nat. Photonics*, 2015, **9**, 174–179.

4 T. Kumari, S. M. Lee, S. Kang, S. Chen and C. Yang, *Energy Environ. Sci.*, 2017, **10**, 258–265.

5 S. Günes, H. Neugebauer and N. S. Sariciftci, *Chem. Rev.*, 2007, **107**, 1324–1338.

6 C. J. Brabec, S. Gowrisanker, J. J. M. Halls, D. Laird, S. Jia and S. P. Williams, *Adv. Mater.*, 2010, **22**, 3839–3856.

7 B. D. Mühlbacher, M. Scharber, M. Morana, Z. Zhu, D. Waller, R. Gaudiana and C. Brabec, *Adv. Mater.*, 2006, **18**, 2884–2889.

8 P. T. Boudreault, A. Najari and M. Leclerc, *Chem. Mater.*, 2011, **23**, 456–469.

9 W. Cai, X. Gong and Y. Cao, *Sol. Energy Mater. Sol. Cells*, 2010, **94**, 114–127.

10 M. C. Scharber, D. Mühlbacher, M. Koppe, D. Patrick, C. Waldauf, A. J. Heeger and C. J. Brabec, *Adv. Mater.*, 2006, **18**, 789–794.

11 K. Kawashima, Y. Tamai, H. Ohkita, I. Osaka and K. Takimiya, *Nat. Commun.*, 2015, **6**, 10085.

12 K. Kawashima, T. Fukuhara, Y. Suda, Y. Suzuki, T. Koganezawa, H. Yoshida, H. Ohkita, I. Osaka and K. Takimiya, *J. Am. Chem. Soc.*, 2016, **138**, 10265–10275.

13 I. Osaka and K. Takimiya, *Adv. Mater.*, 2017, **29**, 1605218.

14 J. Peet, A. J. Heeger and G. C. Bazan, *Acc. Chem. Res.*, 2009, **42**, 1700–1708.

15 J. Chen and Y. Cao, *Acc. Chem. Res.*, 2009, **42**, 1709–1718.

16 J. Du, M. C. Biewer and M. C. Stefan, *J. Mater. Chem. A*, 2016, **4**, 15771–15787.

17 Z. Chen, P. Cai, J. Chen, X. Liu, L. Zhang and L. Lan, *Adv. Mater.*, 2014, **26**, 2586–2591.

18 Y. Liu, J. Zhao, Z. Li, C. Mu, W. Ma, H. Hu, K. Jiang and H. Lin, *Nat. Commun.*, 2014, **5**, 5293.

19 Q. Zhang, M. A. Kelly, N. Bauer and W. You, *Acc. Chem. Res.*, 2017, **50**, 2401–2409.

20 W. Chen and F. He, *Polym. Chem.*, 2018, **9**, 940–947.

21 Z. Fei and M. Heeney, *J. Mater. Chem. C*, 2015, **3**, 265–275.

22 A. Wakamiya, T. Taniguchi and S. Yamaguchi, *Angew. Chem., Int. Ed.*, 2006, **45**, 3170–3173.

23 H. Nishimura, N. Ishida, A. Shimazaki, A. Wakamiya, A. Saeki, L. T. Scott and Y. Murata, *J. Am. Chem. Soc.*, 2015, **137**, 15656–15659.

24 C. Dou, Z. Ding, Z. Zhang, Z. Xie, J. Liu and L. Wang, *Angew. Chem., Int. Ed.*, 2015, **54**, 3648–3652.

25 C. Dou, X. Long, Z. Ding, Z. Xie, J. Liu and L. Wang, *Angew. Chem., Int. Ed.*, 2016, **55**, 1436–1440.

26 H. Shimogawa, O. Yoshikawa, Y. Aramaki, M. Murata, A. Wakamiya and Y. Murata, *Chem.–Eur. J.*, 2017, **23**, 3784–3791.

27 H. Shimogawa, M. Endo, T. Taniguchi, Y. Nakaike, M. Kawaraya, H. Segawa, Y. Murata and A. Wakamiya, *Bull. Chem. Soc. Jpn.*, 2017, **90**, 441–450.

28 H. Shimogawa, M. Endo, Y. Nakaike, Y. Murata and A. Wakamiya, *Chem. Lett.*, 2017, **46**, 715–718.

29 H. Shimogawa, Y. Murata and A. Wakamiya, *Org. Lett.*, 2018, **20**, 5135–5138.

30 T. C. Parker, D. G. Patel, K. Moudgil, S. Barlow, C. Risko, J. L. Brédas, J. R. Reynolds and S. R. Marder, *Mater. Horiz.*, 2015, **2**, 22–36.

31 Y. Wang and T. Michinobu, *J. Mater. Chem. C*, 2016, **4**, 6200–6214.

32 M. Satou, K. Uchinaga, A. Wakamiya and Y. Murata, *Chem. Lett.*, 2014, **43**, 1386–1388.

33 M. Satou, T. Nakamura, Y. Aramaki, S. Okazaki, M. Murata, A. Wakamiya and Y. Murata, *Chem. Lett.*, 2016, **45**, 892–894.

34 T. Nakamura, S. Okazaki, N. Arakawa, M. Satou and M. Endo, *J. Photopolym. Sci. Technol.*, 2017, **30**, 561–568.

35 J. Subbiah, B. Purushothaman, M. Chen, T. Qin, M. Gao, D. Vak, F. H. Scholes, X. Chen, S. E. Watkins, G. J. Wilson, A. B. Holmes, W. W. H. Wong and D. J. Jones, *Adv. Mater.*, 2015, **27**, 702–705.

36 M. Gao, J. Subbiah, P. B. Geraghty, M. Chen, B. Purushothaman, X. Chen, T. Qin, D. Vak, F. H. Scholes, S. E. Watkins, M. Skidmore, G. J. Wilson, A. B. Holmes, D. J. Jones and W. W. H. Wong, *Chem. Mater.*, 2016, **28**, 3481–3487.

37 M. J. Frisch, G. W. Trucks, H. B. Schlegel, G. E. Scuseria, M. A. Robb, J. R. Cheeseman, G. Scalmani, V. Barone, G. A. Petersson, H. Nakatsuji, X. Li, M. Caricato, A. Marenich, J. Bloino, B. G. Janesko, R. Gomperts, B. Mennucci, H. P. Hratchian, J. V. Ortiz, A. F. Izmaylov, J. L. Sonnenberg, D. Williams-Young, F. Ding, F. Lipparini, F. Egidi, J. Goings, B. Peng, A. Petrone, T. Henderson, D. Ranasinghe, V. G. Zakrzewski, J. Gao, N. Rega, G. Zheng, W. Liang, M. Hada, M. Ehara, K. Toyota, R. Fukuda, J. Hasegawa, M. Ishida, T. Nakajima, Y. Honda, O. Kitao, H. Nakai, T. Vreven, K. Throssell, J. A. Montgomery Jr, J. E. Peralta, F. Ogliaro, M. Bearpark, J. J. Heyd, E. Brothers, K. N. Kudin, V. N. Staroverov, T. Keith, R. Kobayashi, J. Normand, K. Raghavachari, A. Rendell, J. C. Burant, S. S. Iyengar, J. Tomasi, M. Cossi, J. M. Millam, M. Klene, C. Adamo, R. Cammi, J. W. Ochterski, R. L. Martin, K. Morokuma, O. Farkas, J. B. Foresman, and D. J. Fox, *Gaussian 09, Revision C.01*, Gaussian, Inc., Wallingford CT, 2016.

38 B. W. D'Andrade, S. Datta, S. R. Forrest, P. Djurovich, E. Polikarpov and M. E. Thompson, *Org. Electron.*, 2005, **6**, 11–20.

39 C. V. Hoven, X. D. Dang, R. C. Coffin, J. Peet, T. Q. Nguyen and G. C. Bazan, *Adv. Mater.*, 2010, **22**, 63–66.